Electronic Supplementary Information (ESI) Materials Horizons.
This journal is © The Royal Society of Chemistry 2024

Electronic Supplementary Information

Epsilon-near-zero thin films in a dual-functional system for thermal infrared camouflage and thermal management within the atmospheric window

Pei-Chi Hsieh[a], Sih-Wei Chang[a], Wei-Hsuan Kung[a], Tzu-Chieh Hsiao[a], and Hsuen-Li Chen*[a,b]

[a] Department of Materials Science and Engineering, National Taiwan University, Taipei 10617, Taiwan.

[b] Center of Atomic Initiative for New Materials, National Taiwan University, Taipei 10617, Taiwan

*Corresponding author. E-mail: hsuenlichen@ntu.edu.tw

The mechanism of the Berreman mode:

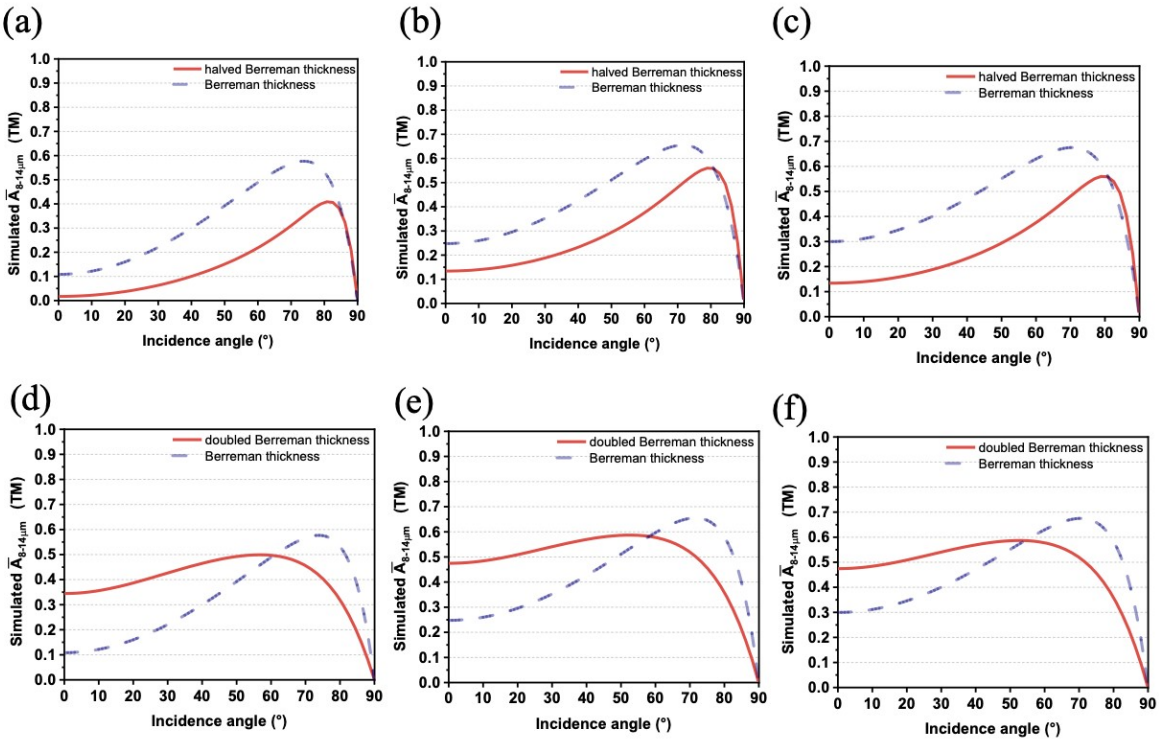

Figure S1. Optical simulated average angle-resolved absorptance for the TM polarization in the LWIR wavelength range of 8–14 μm of the ENZ thin film stack, with (a-c) halved and (d-f) doubled Berreman thickness for each ENZ material layer, deposited on a bottom layer of (a, d) Au, (b, e) metallic glass I, and (c, f) metallic glass II films on Si wafer. (The optical simulated simulation results for the Berreman thickness are shown as dashed lines)

Optical simulated angle-resolved absorptance spectrum:

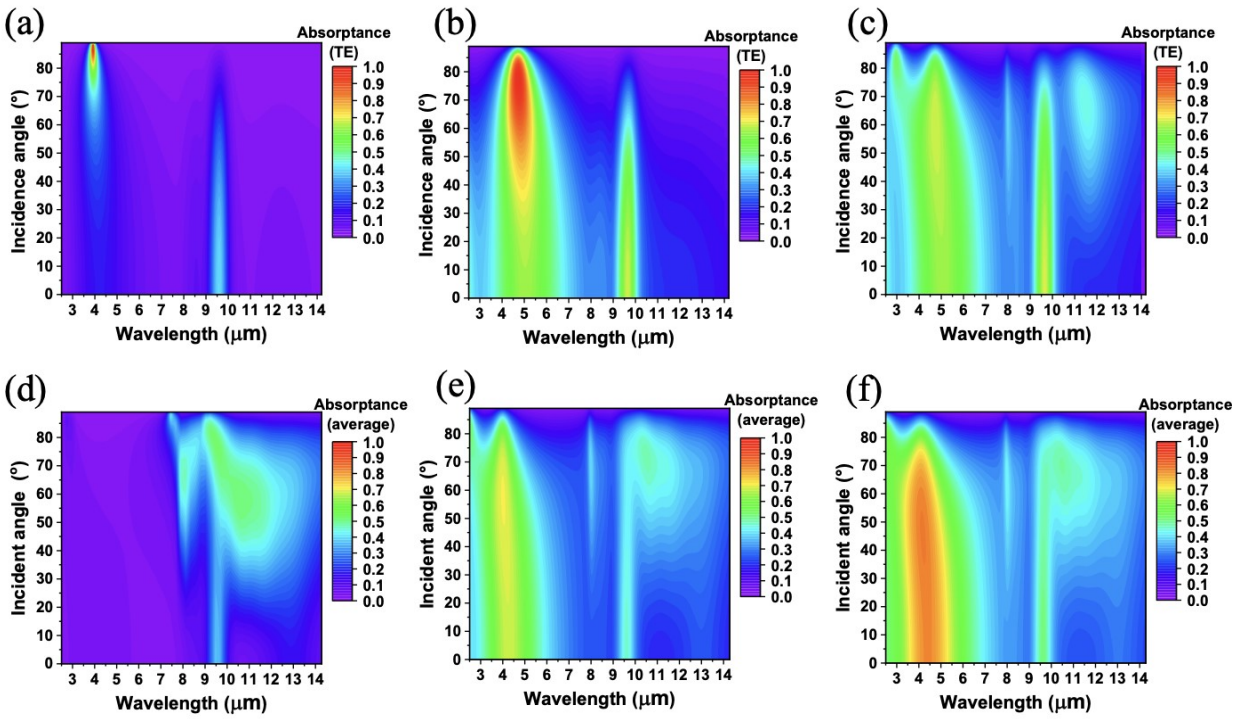

Figure S2. Optical simulated angle-resolved absorptance spectrum for (a-c) TE polarization, (d-f) the average polarization of the ENZ thin film stack deposited on a base bottom layer of (a, d) Au, (b, e) metallic glass I, and (c, f) metallic glass II films on Si wafer.

Optical admittance diagram:

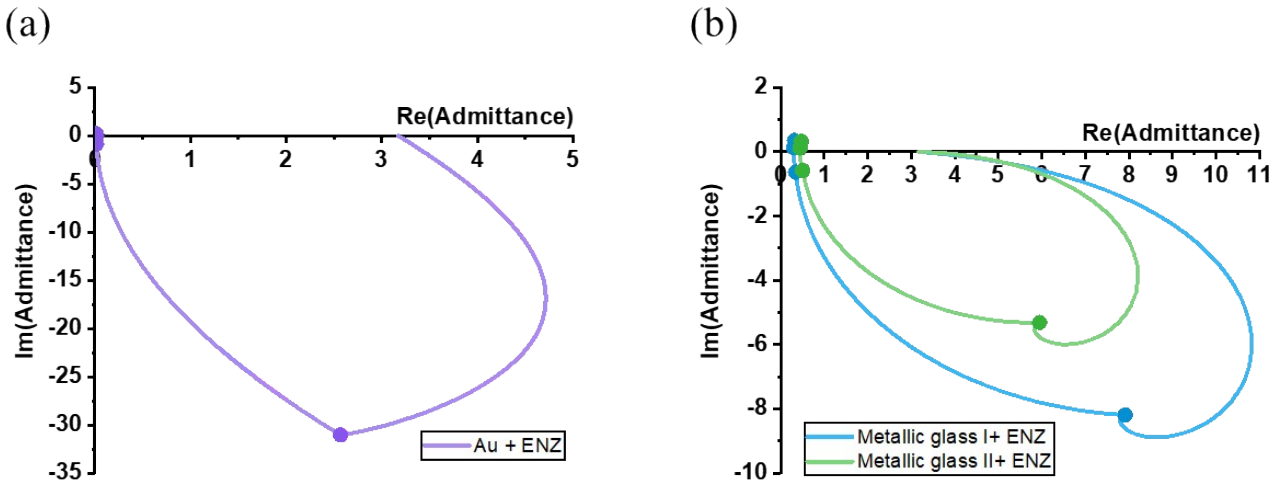

Figure S3. Optical admittance diagram at the wavelength of 4.3 μm of ENZ thin film stack deposited on a bottom layer of **(a)** Au and **(b)** metallic glass I and metallic glass II films on Si wafer.

Calculations of radiative cooling power:

The energy balance equation and net heat exchange (P_{net}) of a radiative cooling system can be expressed as [1, 2]:

$$P_{net} = P_{rad}(T_{surf}) - P_{atm}(T_{atm}) - P_{con}(T_{surf},T_{amb}) \quad \text{(S1)}$$

P_{rad} represents the power radiated by the surface of the radiative cooler, expressed as

$$P_{rad}(T_{surf}) = \int d\Omega \cos\theta \int_0^{\infty} d\lambda\, B(T_{surf},\lambda)\, \varepsilon(\lambda,\theta) \quad \text{(S2)}$$

where T_{surf} is the equilibrium temperature of the surface of the radiative cooler, $\varepsilon(\lambda,\theta)$ is the emissivity of the radiative cooler, and B is the spectral radiance of blackbody radiation.

P_{atm} represents the absorbed thermal radiation power emitted from the atmosphere by the top surface in the heat transfer model, expressed as:

$$P_{atm}(T_{atm}) = \int d\Omega \cos\theta \int_0^{\infty} d\lambda\, B(T_{atm},\lambda)\, \varepsilon(\lambda,\theta)\, \varepsilon_{atm}(\lambda,\theta) \quad \text{(S3)}$$

where T_{atm} is the temperature of the atmosphere assuming the same as the temperature of the ambient; $\varepsilon_{atm}(\lambda,\theta)$is the angular emissivity of the atmosphere, expressed as:

$$\varepsilon_{atm}(\lambda,\theta) = 1 - t(\lambda)^{\frac{1}{\cos\theta}} \quad \text{(S4)}$$

where $t(\lambda)$ is the transmittance of the atmosphere in the zenith direction.

P_{con} represents the power exchange by the conductive and convective heat between the top surface in the heat transfer model and the surroundings, expressed as

$$P_{con}(T_{surf},T_{amb}) = h(T_{amb} - T_{surf}) \quad \text{(S5)}$$

where h is the conductive and convective heat exchange coefficient and T_{amb} is the ambient temperature. The experience formula for h can be expressed as

$$h = 3.3 + 2v \quad \text{(S6)}$$

where v is the wind velocity in a unit of m s^{-1}.

In our study, the samples exhibited angle-dependent emissivity. To simplify the calculation, we calculated the average emissivity from the angle-dependent emissivity of the sample and then used the equations to obtain the power exchange (P_{net}) of the radiative cooling system. The average emissivity was calculated from the angle-dependent emissivity of the sample using the following equation:

$$\bar{\varepsilon}(\lambda) = \frac{\int d\Omega \cos\theta \, \varepsilon(\lambda,\theta)}{\int d\Omega \cos\theta} \quad \text{(S7)}$$

A schematic of the angle-dependent emissivity of the sample is shown in Figure S2

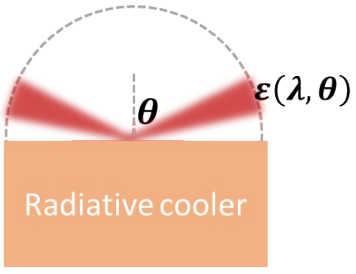

Figure S4. Schematic diagram of the angle-dependent emissivity of the sample.

Optical simulated absorptance spectrum under different configurations of TiO_2, Al_2O_3, and SiO_2 thin films:

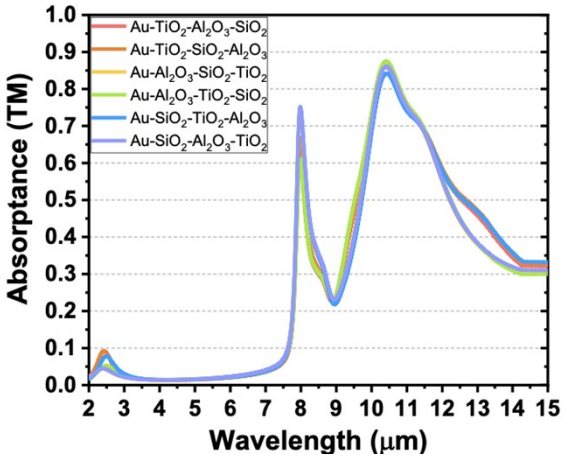

Figure S5. Optical simulated absorptance spectrum under TM polarization of different configurations of TiO_2, Al_2O_3, and SiO_2 thin films on the base metal layer of Au film with an incident light angle of 80^o.

Table S1. Average absorbance under TM polarization within the wavelength range of LWIR atmospheric window (8-14 μm) of different configurations of TiO_2, Al_2O_3, and SiO_2 thin films

Different configuration	$\overline{A}_{8-14\mu m}$ (TM) at an incident light angle of 80^o
Au-TiO_2-Al_2O_3-SiO_2	0.533
Au-TiO_2-SiO_2-Al_2O_3	0.533
Au-Al_2O_3-SiO_2-TiO_2	0.514
Au-Al_2O_3-TiO_2-SiO_2	0.519
Au-SiO_2-TiO_2-Al_2O_3	0.529
Au-SiO_2-Al_2O_3-TiO_2	0.515

on the base metal layer of Au film with an incident light angle of 80^o

Calculation of the apparent temperature similarity in the camouflage demonstration:

One approach to determine the apparent temperature similarity between the target and background is to calculate the Euclidean distance of the points in thermal infrared images [3-7]. In this study, red, green, and blue (RGB) color spaces were utilized, where the value of each color ranged from 0 to 255. For two specified points in thermal infrared images, their colors in the RGB color space are denoted as (R_1, G_1, B_1) and (R_2, G_2, B_2). The similarity between these two points can be obtained using the following equation:

$$Similarity(\%) = \left(1 - \frac{\sqrt{\left(\frac{R_1 - R_2}{255}\right)^2 + \left(\frac{G_1 - G_2}{255}\right)^2 + \left(\frac{B_1 - B_2}{255}\right)^2}}{3}\right) \times 100\% \quad \text{(S8)}$$

References

1 J. Kischkat, S. Peters, B. Gruska, M. Semtsiv, M. Chashnikova, M. Klinkmüller, O. Fedosenko, S. Machulik, A. Aleksandrova, and G. Monastyrskyi, "Mid-infrared optical properties of thin films of aluminum oxide, titanium dioxide, silicon dioxide, aluminum nitride, and silicon nitride," *Applied optics*, 2012, **51**, no. 28, pp. 6789-6798.

2 R. L. Olmon, B. Slovick, T. W. Johnson, D. Shelton, S.-H. Oh, G. D. Boreman, and M. B. Raschke, "Optical dielectric function of gold," *Physical Review B*, 2012, **86**, no. 23, pp. 235147.

3 A. P. Raman, M. A. Anoma, L. Zhu, E. Rephaeli, and S. Fan, "Passive radiative cooling below ambient air temperature under direct sunlight," *Nature*, 2014, **515**, no. 7528, pp. 540-544.

4 B. Zhao, M. Hu, X. Ao, N. Chen, and G. Pei, "Radiative cooling: A review of fundamentals, materials, applications, and prospects," *Applied energy*, 2019, **236**, pp. 489-513.

5 N. Selvarasu, A. Nachiappan, and N. Nandhitha, "Abnormality detection from medical thermographs in human using Euclidean distance based color image segmentation." pp. 73-75.

6 K. R. Smith, V. Cadena, J. A. Endler, M. R. Kearney, W. P. Porter, and D. Stuart-Fox, "Color change for thermoregulation versus camouflage in free-ranging lizards," *The American Naturalist*, 2016, **188**, no. 6, pp. 668-678.

7 T. Woo, X. Liang, D. A. Evans, O. Fernandez, F. Kretschmer, S. Reiter, and G. Laurent, "The. dynamics of pattern matching in camouflaging cuttlefish," *Nature*, 2023, **619**, no. 7968, pp. 122-128.